JOURNAL OF Materials CHEMISTRY

Syntheses, structures and properties of some osmates(IV,V) adopting the pyrochlore and weberite structures

J. Reading, C. S. Knee and M. T. Weller*

Department of Chemistry, University of Southampton, Southampton, UK SO17 1BJ. E-mail: mtw@soton.ac.uk

Received 7th February 2002, Accepted 14th May 2002
First published as an Advance Article on the web 14th June 2002

Samples of the complex osmates $Ca_2Os_2O_7$, $Tl_2Os_2O_{7-x}$ and $Pb_2Os_2O_{7-x}$ have been obtained by direct reaction of the component oxides in sealed tubes. The structures and compositions of these materials have been investigated by powder neutron and X-ray diffraction at room temperature and through variable temperature studies. $Ca_2Os_2O_7$ adopts a stoichiometric, orthorhombic weberite structure but the distortion of the OsO_6 octahedra and eightfold Ca–O co-ordinations decrease with increasing temperature indicating that this material lies close to the weberite/pyrochlore phase boundary. The lead and thallium phases adopt oxygen deficient, cubic pyrochlore structures under the synthesis conditions employed though no evidence was found of cation non-stoichiometry. Preliminary measurements of the electronic properties of weberite $Ca_2Os_2O_7$ are also reported and discussed in comparison with the lead, thallium, cadmium and mercury osmate pyrochlores.

Introduction

Pyrochlores containing the 2nd and 3rd row transition metals have recently become of considerable interest due to the unusual electronic, ionic and magnetic properties they exhibit.[1] Examples include the molybdate(IV) pyrochlores of the type $Ln_2Mo_2O_7$ which have been shown to be excellent mixed ionic/electronic conductors[2,3] and the thallium ruthenates $Tl_{2-x}Ru_{2-y}O_{7-z}$, studied in detail by Takeda *et al.*.[4] The thallium ruthenates exhibit complex electronic and structural behaviour, in this case dependent on composition, including metal–insulator transitions and magnetoresistive properties. The unusual oxidation state (in the solid state) Re(V) may be obtained in the oxide pyrochlore structure within $Cd_2Re_2O_7$; this compound shows a number of complex electronic and structural behaviours culminating with a transition to superconducting behaviour below 1.4 K.[5]

The pyrochlore structure is widely adopted by materials of the stoichiometry $A_2B_2O_7$ where B is a tetravalent or pentavalent species and A, therefore, respectively trivalent or divalent. The structure, which can be considered to be based on an anion deficient fluorite structure or, alternatively, in terms of BO_6 octahedra linked through all vertices, Fig. 1, has been discussed and reviewed in detail by Subramanian *et al.*;[1] the A type cations all have distorted (6 + 2) co-ordination to oxygen. In this polyhedral description one oxygen, O2, does not form part of the BO_6 framework interacting solely with the A-type cations. The ability of the structure to accommodate high levels of oxide ion deficiencies on the O2 site, producing at the extreme $A_2B_2O_6$[] where [] represents a vacancy, allows for the formation of many mixed valence pyrochlores as has been reported, for example, in systems such as $Sr_2Os_2O_{6.4}$[6] and $Bi_2Rh_2O_{6.8}$.[7]

The weberite structure, also adopted by some materials of

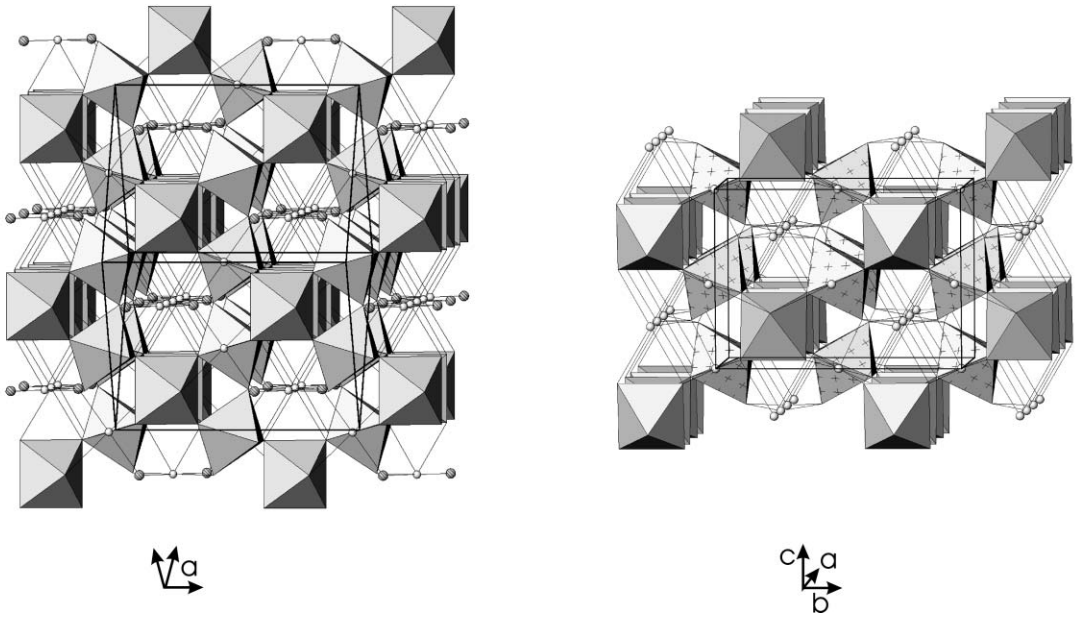

Fig. 1 The pyrochlore (left) and weberite (right) structures shown as connected BO_6 octahedra viewed along the main 8-ring channels. The A-type cation positions are shown are pale grey spheres, the O2 sites in the pyrochlore structure as darker spheres and the unit cells are outlined.

 DOI: 10.1039/b201410f

the stoichiometry $A_2B_2O_7$, *e.g.* $Sr_2Sb_2O_7$[8] is closely related to the pyrochlore structure in that the B type cations adopt octahedral co-ordination to oxygen but in this structure only half the octahedra have all vertices linked to neighbouring BO_6 units, the remainder are linked through four vertices only, Fig. 1, and all oxide ions form part of the BO_6 units of the framework. The two different A cation environments still involve co-ordination to eight oxide ions that are best described in both cases as strongly distorted cubic. In one case the cube is deformed by contraction along a C_4 axis producing 4 + 4 co-ordination and in the other by contraction along a C_3 axis producing hexagonal bipyramidal co-ordination though the equatorial oxygen ion plane is slightly puckered.

The phase behaviour of $A_2Sb_2O_7$ phases as a function of A and adoption of pyrochlore or weberite structure has been studied in detail by Knop *et al.*[9] For these systems $Ca_2Sb_2O_7$ lies at the borderline of phase stability occurring in both pyrochlore or weberite forms depending on the pressure used during phase formation, with high pressures favouring pyrochlore formation. For A = Cd the pyrochlore structure readily forms indicating that increased covalency in the A–O bond promotes the pyrochlore arrangement.

While $(A_2^{2+}B_2^{5+})O_7$ systems have been studied in detail for B = Sb, Nb, Ta, osmium(v) systems have been less well studied with the exception of $A_2Os_2O_7$, A = Cd, Hg.[10–13] $Cd_2Os_2O_7$ undergoes a continuous Slater-like transition at 225 K, where the formation of an antiferromagnetic state and formal doubling of the unit cell, with minor structural changes, results in the slow opening of a semi-conducting band gap. We have recently reported upon $Hg_2Os_2O_7$, which shows weaker electronic and magnetic transitions near 88 K.[13] Calcium osmate pyrochlores have also been reported in the literature though there is a great deal of confusion over the stoichiometry, structure and properties of these compounds. Both Chamberland[14,15] and Shaplygrin[16] have reported formation of a stoichiometric phase of the composition $Ca_2Os_2O_7$ using differing routes. Decomposition of $CaOsOH_6$ leads to a cubic phase while direct reaction of CaO and OsO_2 at 1000 °C results in a tetragonal phase with lattice parameters given as 10.12 and 10.69 Å. An orthorhombic phase, of undetermined stoichiometry and purity, can also be obtained by thermal decomposition of $CaOsO_3$[16] while reaction of CaO and OsO_2 under high pressure leads to a cubic, calcium-deficient phase $Ca_{1.7}Os_2O_7$.[17]

Other osmate pyrochlores briefly reported in the literature are $Pb_2Os_2O_{7-x}$.[18,19] and $Tl_2Os_2O_7$[20] but these have been poorly defined in terms of stoichiometry and, for the thallium material, have only been obtained under high pressure synthesis conditions. In this paper we report on the synthesis under ambient pressure of pyrochlores of the compositions, $Pb_2Os_2O_{7-x}$ and $Tl_2Os_2O_{7-x}$ and of $Ca_2Os_2O_7$, which adopts the weberite structure when synthesised under ambient pressure conditions.

Experimental

Synthesis

Samples of $Tl_2Os_2O_{7-x}$, $Pb_2Os_2O_{7-x}$ and $Ca_2Os_2O_7$ were prepared by grinding together the appropriate stoichiometric mixtures of high purity Tl_2O_3 (99.9%), PbO (99.9+%), CaO (99+%), Os (99.8%) OsO_2 (99.99%) and OsO_4 (99.95%). Tl_2O_3 and PbO were pre-dried at 300 °C for 1 day before use. CaO was prepared by heating $CaCO_3$ at 1000 °C for 1 week. $Tl_2Os_2O_{7-x}$ was synthesised using Tl_2O_3 and OsO_2. For $Pb_2Os_2O_{7-x}$ and $Ca_2Os_2O_7$ appropriate mixtures of PbO, CaO, OsO_4 and Os were used. Stoichiometric mixtures were loaded into silica ampoules and sealed under vacuum; in the case of $Pb_2Os_2O_{7-x}$ and $Ca_2Os_2O_7$ the end of the ampoule was immersed in liquid nitrogen to avoid osmium loss due to the volatility of OsO_4. The synthesis temperatures for $Tl_2Os_2O_{7-x}$ and $Pb_2Os_2O_{7-x}$ were 500 and 800 °C respectively, with a reaction period of 1 day in each case. The precursor mixture for $Ca_2Os_2O_7$ was fired initially at 800 °C for 2 days and then at 1000 °C for 1 day, with an intermediate sample regrinding and resealing during the course of the reaction.

Powder X-ray diffraction data were recorded from the products using a Siemens D5000 diffractometer operating with Cu $K_{\alpha 1}$ radiation. The $Tl_2Os_2O_{7-x}$ and $Pb_2Os_2O_{7-x}$ patterns were consistent with cubic pyrochlore phase materials with the exception of a small amount of Tl_2O_3 impurity (<3%) in $Tl_2Os_2O_{7-x}$. $Ca_2Os_2O_7$ showed a more complex pattern indicative of an orthorhombic unit cell with small distortions from the cubic cell of pyrochlore. Comparison of this unit cell to those in the literature for distorted pyrochlores and related phases showed that the data could be indexed completely on a cell of approximate dimensions 7.3 × 7.5 × 10.2 Å (corresponding roughly to $a_p/\sqrt{2} \times a_p/\sqrt{2} \times a_p$ where a_p is the cubic, pyrochlore lattice parameter); these values are similar to those found for $Ca_2Sb_2O_7$ with the weberite structure. Heating this material to 600 °C *in situ* on a Bruker D8 diffractometer, using the HTK stage, showed that the structure remains orthorhombic to this temperature and does not undergo transformation to the cubic pyrochlore structure prior to its decomposition that occurs above 700 °C in air.

Powder neutron diffraction data were collected on the POLARIS diffractometer on ISIS, Rutherford–Appleton Laboratory, for periods ranging from 1 to 2 hours; data were obtained from $Ca_2Os_2O_7$ at four temperatures between 2 and 400 K, from $Tl_2Os_2O_{7-x}$ at 2 K and room temperature and from $Pb_2Os_2O_{7-x}$ at room temperature only. Only data from the back-scattering bank were used in the refinement; large *d*-spacing data obtained in the low angle bank were inspected for the presence of magnetic reflection but none was seen for any of the samples at any temperature. The GSAS program suite was used for the structure refinement.[21]

Data from $Pb_2Os_2O_{7-x}$ and $Tl_2Os_2O_{7-x}$ could be fully indexed using a cubic unit cell except for a few weak reflections from the vanadium can and, for the thallium-containing sample, a small level of Tl_2O_3 impurity. Refinement of the structures for these data sets was carried out using the normal pyrochlore crystallographic description in the space group $Fd\bar{3}m$. Refinements initially converged rapidly in each case with the use of isotropic thermal displacement parameters (TDP) for all atoms but inspection of the refined values showed unreasonably large TDP values for the O2 site; for example with $Tl_2Os_2O_{7-x}$ U_{iso} was 0.07 $Å^2$ for O2 compared with 0.002–0.006 $Å^2$ for the other three atom sites. Thus in the later stages of the refinement the occupancy factors for the oxygen and, for completeness, the lead/thallium sub-lattices were probed. The O2 site occupancy refined to a value significantly below unity, in the range 0.6–0.8 in both cases, but the thallium and lead site occupancies refined to values of 1.02(3) and 1.00(2), respectively, demonstrating that this site was fully occupied. The final stages of the refinement maintained the site occupancies of all atoms at unity except for O2 and included anisotropic thermal displacement parameters for all atoms. The additional phases, vanadium and Tl_2O_3 were included as necessary. Final refined atomic parameters are summarised as part of Tables 1 and 2 and derived bond lengths and angles of significance are given in Table 3. The use of isotropic or anisotropic TDPs in the models had little effect upon the key positional parameters showing acceptably low correlations in these parameters for the cubic structure with low parameter numbers and well resolved reflections

For $Ca_2Os_2O_7$ the data collected at all temperatures were consistent with adoption of the weberite structure and the co-ordinate description for $Sr_2Sb_2O_7$, given by Groen and Ijdo,[8] was used as a starting model. The structural model for the 2 K data was refined initially and iterations converged

Table 1 Refined structural data for $Ca_2Os_2O_7$ as a function of temperature. Orthorhombic, space group *Imma*. Ca1 on (0,0,0), Ca2 on ($\frac{1}{4}$, $\frac{1}{4}$,$\frac{1}{2}$), Os1 on ($\frac{1}{4}$, $\frac{1}{4}$, $\frac{1}{4}$), Os2 on (0,0,$\frac{1}{2}$), O1 on (0, $\frac{1}{4}$,*z*), O2 on (0,*y*,*z*) and O3 on (*x*,*y*,*z*). *U* values given are $100U_{iso}/Å^2$. Esds are given in parentheses

T/K	*a*/Å	*b*/Å	*c*/Å	O1 *z*	O2 *y*	O2 *z*	O3 *x*	O3 *y*	O3 *z*	Ca1 *U*	Ca2 *U*	Os1 *U*	Os2 *U*	O1 *U*	O2 *U*	O3 *U*	R_{F2}	R_{wp}	χ^2
100	7.2062(2)	10.1089(2)	7.3746(2)	0.1625(4)	0.4038(2)	0.7279(2)	0.2059(2)	0.3834(1)	0.4356(2)	0.25(5)	0.21(6)	0.04(2)	0.00(2)	0.55(4)	0.26(3)	0.21(2)	2.70	3.27	6.27
200	7.2076(2)	10.1135(2)	7.3775(2)	0.1615(4)	0.4037(2)	0.7280(20	0.2057(2)	0.3833(10	0.4354(2)	0.50(6)	0.47(7)	0.08(3)	0.09(2)	0.75(40	0.39(3)	0.33(2)	3.47	3.22	5.27
298	7.2104(2)	10.1211(3)	7.3813(2)	0.1597(5)	0.4036(2)	0.7282(3)	0.2051(2)	0.3830(2)	0.4350(2)	0.80(8)	0.74(8)	0.15(3)	0.15(3)	0.94(5)	0.54(4)	0.48(2)	3.81	3.44	2.84
400	7.2131(2)	10.1279(3)	7.3853(2)	0.1578(4)	0.4036(2)	0.7283(3)	0.2041(2)	0.3830(2)	0.4348(2)	1.02(8)	1.06(9)	0.19(3)	0.20(3)	1.04(5)	0.74(4)	0.62(2)	4.11	3.16	5.02

rapidly. Final stages of the refinement included all atomic positions and isotropic thermal displacement parameters. The increased complexity of the weberite structure, in comparison with pyrochlore, does not justify the use of anisotropic TDPs for the medium resolution POLARIS diffractometer. Data from the higher temperature runs were analysed using an identical methodology. Final refined atomic co-ordinates and fit parameters obtained, as a function of temperature, are summarised in Tables 1 and 2 and the final profile fit obtained to the room temperature data shown in Fig. 2. Derived bond lengths for this material are presented as a function of temperature in a graphical manner in Fig. 3 and 4.

CCDC reference number 182356.

See http://www.rsc.org/suppdata/jm/b2/b201410f/ for powder diffraction data in CIF or other electronic format.

Resistivity measurement

Resistivity data were collected from the weberite form $Ca_2Os_2O_7$ using standard four probe methods. A bar of material (approximately 2 × 5 × 10 mm) was pressed under 10 tonnes and sintered at 500 °C and silver electrodes painted on to it. Data were collected between 200 and 445 K. For the thallium and lead systems room temperature measurements only were undertaken and confirmed high conductivity, in the metallic regime, with resistivity values of 10^{-2} Ω cm.

Results and discussion

Structural and compositional derivatives of the pyrochlore structure are relatively rare in comparison, for example, to those found for perovskites, where anion defect structures and non-cubic systems are prevalent. However, models have been derived discussing phase stability as a function of, for example, ionic radii and covalency. Pannetier and Lucas have analysed the pyrochlore structure in terms of the polyhedra around the A and B cation types, the strength and covalency of the A–O' bond and similarities with the SiO_2 structure in terms of distorted derivatives.[22]

$Ca_2Os_2O_7$

$Ca_2Os_2O_7$ adopts the weberite structure when synthesised under ambient pressure conditions rather than the distorted pyrochlore structures reported previously for this material. The adoption of this structure type presumably results from the electropositivity and co-ordination preferences of calcium as the osmate octahedra are similar in the two structure types. A comparison of the co-ordination environments of calcium in $Ca_2Os_2O_7$ (weberite) and cadmium in $Cd_2Os_2O_7$ (pyrochlore) is shown in Fig. 5; accepted ionic radii for these cations in 8-fold co-ordination are $r\,(Ca^{2+}) = 1.12$ Å and $r\,(Cd^{2+}) = 1.10$ Å so similar bond lengths would be expected for these two ions. Bond valence calculations for the cations are summarised in Table 3 and confirm this material as $Ca^{2+}{}_2Os^{5+}{}_2O_7$.[23]

In both materials the cations are 8-co-ordinate to oxygen as would be expected for structures based on the fluorite sub-lattice; these co-ordination geometries are, however, strongly distorted from cubic in each case. The most noticeable feature of the A cation co-ordination in the pyrochlore structure is the very short A–O2 distance; this is 2.196 Å for Cd–O in $Cd_2Os_2O_7$ compared with the sum of the ionic radii, 2.36 Å. Clearly for d^{10} species such as Cd^{2+}, Hg^{2+} and Ag^{2+} which prefer linear co-ordinations this structural motif helps stabilise the pyrochlore structure. In the weberite structure one of the A cation sites has a similar geometry though the Ca–O distance is less obviously shortened, Ca–O is 2.231 Å, and the other site has a much more regular 4+4 geometry with the shortest Ca–O interaction at 2.386 Å. This tendency to avoid very short A(Ca)–O distances is reflected in the other reported $Ca_2B_2O_7$

Table 2 Summary of derived atomic, thermal and profile fit parameters for $Pb_2Os_2O_{7-x}$ and $Tl_2Os_2O_{7-x}$ (two temperatures); esds are given in parentheses. Space group $Fd\bar{3}m$. Hg on (½,½,½), Os on (0,0,0), O1 on $(x,\frac{1}{8},\frac{1}{8})$ O2 on $(\frac{3}{8},\frac{3}{8},\frac{3}{8})$

Compound and T/K	a/Å	O1 x	Pb/Tl U_{eq} × 100 Å^2	Os U_{eq} × 100 Å^2	O1 U_{eq} × 100 Å^2	O2 U_{eq} × 100 Å^2	O2 occupancy	R_{wp} (%)	R_p (%)	χ^2
$Pb_2Os_2O_{7-x}$ 298 K	10.35128(3)	0.31961(5)	1.23(1)	0.18(1)	0.65(1)	3.5(1)	0.63(1)	2.40	5.10	1.18
$Tl_2Os_2O_{7-x}$ 2 K	10.27315(5)	0.32077(11)	0.38(20	0.15(2)	0.76(3)	0.59(7)	0.69(2)	1.00	1.74	1.75
$Tl_2Os_2O_{7-x}$ 298 K	10.29218(3)	0.31978(7)	1.02(2)	0.25(1)	0.97(2)	1.35(7)	0.77(1)	3.03	6.17	1.10

Table 3 Selected bond lengths (Å), bond angles (°) and bond valence sums[23] for $Pb_2Os_2O_{7-x}$, $Tl_2Os_2O_{7-x}$ and $Ca_2Os_2O_7$ $Pb_2Os_2O_{7-x}$ and $Tl_2Os_2O_{7-x}$

	Pb	Tl 2 K	Tl 298 K
Pb/Tl–O1	2.6144(3) × 6	2.5862(8)	2.5982(5)
Pb/Tl–O2	2.24112(1)	2.22420(1)	2.22832(1)
Os–O	1.9666(2)	1.9562(4)	1.9560(3)
O–Os–O	92.82(2)	93.27(4)	92.88(3)
Os–O–Os	137.01(3)	136.36(1)	136.92(4)

Bond valence sums at 298 K. (using extrapolated r_0 value of 1.868 for Os(v) based on literature data). $Pb_2Os_2O_{7-x}$ Os 3.94 (using literature value for Os(IV) r_0; value using Os(v) r_0 is 4.60); Pb 2.95 using Pb^{2+} r_0 and 2.45 using Pb^{4+} r_0 assuming full occupancy of O2; values using refined partial occupancy of O2 are 2.43 and 2.01 respectively. $Tl_2Os_2O_{7-x}$ Os 4.06 assuming Os(IV) (4.73 assuming Os(v)). Tl 3.61 assuming Tl^+ 2.28 assuming Tl^{3+} and full occupancy of O2. Using refined occupancy of O2 Tl 3.21 for Tl^+ and 2.04 using Tl^{3+}. $Ca_2Os_2O_7$. Bond valence sums at 298 K. Ca1 2.19, Ca2 1.83 Os1 4.98 Os2 4.79.

phases. Only $Ca_2Sb_2O_7$ formed under 60 kbar pressure is well characterised as a pyrochlore, where pressure presumably favours short Ca–O distances.[9] $Ca_2Nb_2O_7$ and $Ca_2Ta_2O_7$ have been reported in pyrochlore form but these materials tend to contain defects such as non-stoichiometry or the presence of fluoride and hydroxide, which seem to stabilise this structure.

Consideration of the other main structural features of $Ca_2Os_2O_7$ shows that it contains two types of OsO_6 octahedra which both show small distortions from perfect symmetry; bond lengths are shown in Fig. 3. Os(1)O_6 is linked through six vertices to adjacent octahedral units with internal bond angles between 85 and 90° and inter-octahedral angles of 139.4(2) and 135.9(1)°. Os(2)O_6 is linked to four adjacent octahedral OsO_6 units with bond angles of 135.9(1)° and is also moderately distorted with internal angles between 81.7(1) and 98.3(1)°. Overall the levels of distortion in the octahedra are only slightly larger than those found in other osmates confirming that the main driving force for the formation of the weberite structure is probably the co-ordination preferences of the A-type cations rather than those of the B-type cations.

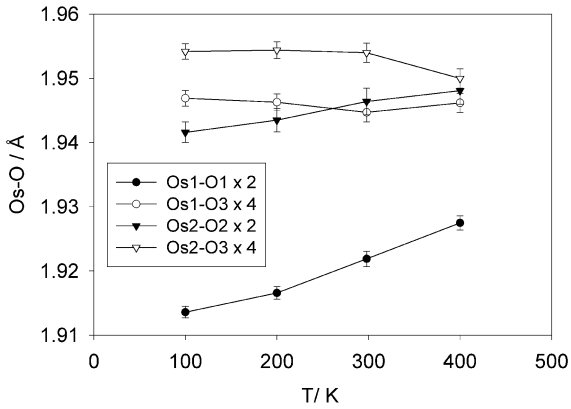

Fig. 3 Variation of the Os–O distances as a function of temperature in $Ca_2Os_2O_7$.

On heating to 600 °C $Ca_2Os_2O_7$ maintains the weberite structure as observed in neutron and X-ray diffraction experiments. Variations in the bond lengths between 2 and 400 K derived from the neutron diffraction data are summarised in

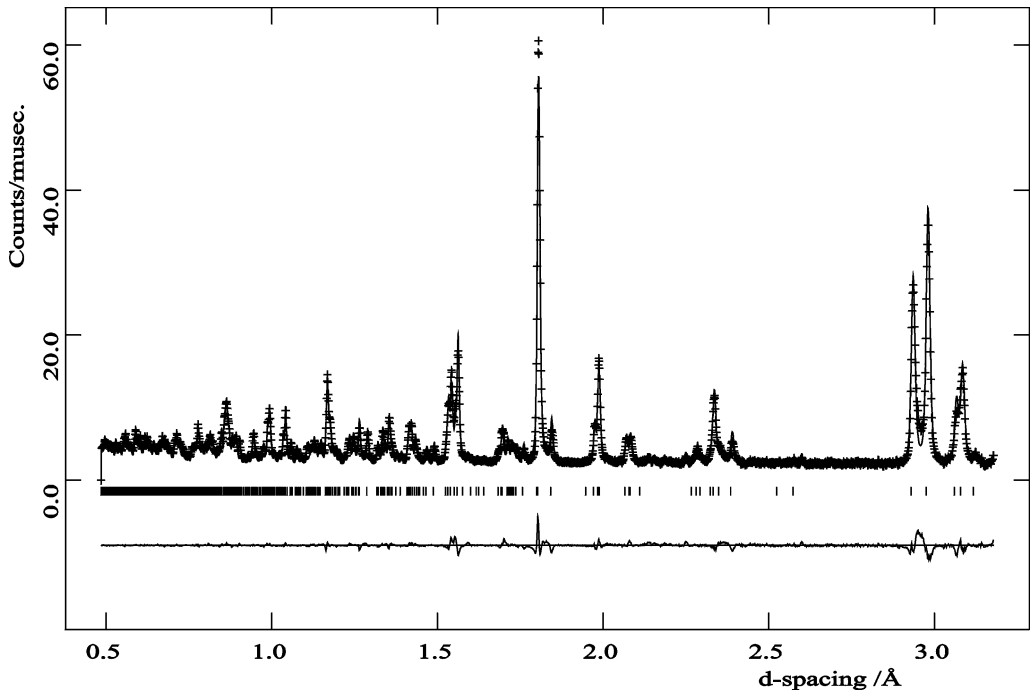

Fig. 2 Final profile fit achieved to the back scattering neutron diffraction data obtained from $Ca_2Os_2O_7$ at room temperature. Cross marks are observed data, upper continuous line the calculated profile and lower continuous line the difference. Tick marks show reflection positions.

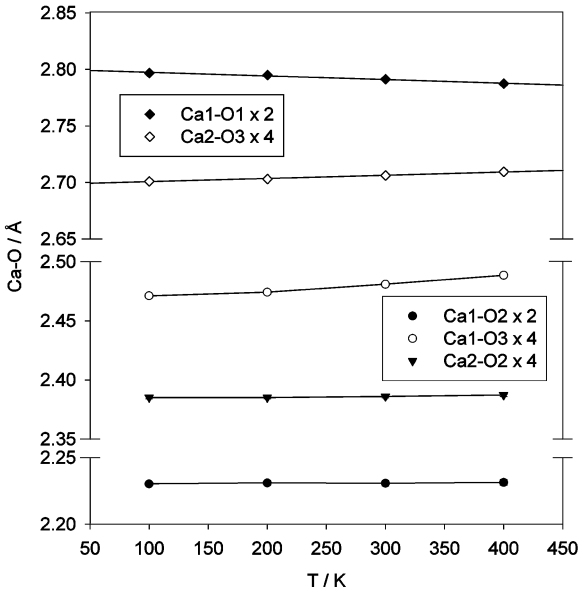

Fig. 4 Variation of the Ca–O distances as a function of temperature in $Ca_2Os_2O_7$.

Fig. 3 and 4. These data show mainly the expected increases in the various bond lengths as a function of temperature though these are not identical. Indications are that the structure becomes more regular at the highest temperatures for example the shortest Os1–O1 bond expands most rapidly approaching the values of the other Os–O bond lengths in this material. Similarly the Ca1 to O3 and O1 distances start to converge, the former shortening significantly between 2 and 400 K while the latter lengthens. The environment of this cation therefore becomes more like the 2 + 6 co-ordination found in pyrochlore. However, extrapolation of these changes to higher temperatures indicates that the more regular co-ordinations of the pyrochlore structure would not be approached until well above the decomposition temperature of $Ca_2Os_2O_7$, near 700 °C in air.

$Tl_2Os_2O_{7-x}$

$Tl_2Os_2O_{7-x}$ adopts a cubic pyrochlore structure, though the material made by direct reaction of Tl_2O_3 and OsO_2, targeting the osmate(IV) $Tl^{3+}{}_2Os^{4+}{}_2O_7$, is oxygen deficient with the stoichiometry $Tl_2Os_2O_{6.69(2)}$ (this composition is obtained from the 2 K neutron diffraction data). The refined composition at room temperature, $Tl_2Os_2O_{6.77(1)}$, was slightly higher, presumably due to parameter correlation problems inherent in the Rietveld analysis in simultaneously refining the occupancy, thermal displacement parameters and background. These compositions are similar to the one obtained by Takeda *et al.*[4] for the corresponding thallium ruthenates synthesised under ambient pressure.

Bond valence calculations for the thallium and osmium sites are given in Table 3 and are dependent on the assumed oxidation states. The value for osmium corresponds most closely to Os(IV) while neither Tl^+ nor Tl^{3+} produces a good fit for the thallium site producing intermediate values, though Tl^{3+} is somewhat better. This material is, therefore, probably correctly represented as $Tl^+{}_{0.23}Tl^{3+}{}_{1.77}Os^{4+}{}_2O_{6.77}$. Reaction under oxygen, especially at high pressure, would be expected to yield stoichiometric $Tl_2Os_2O_7$ as found by Sleight and Gillson[20].

$Pb_2Os_2O_{7-x}$

The structure of $Pb_2Os_2O_{6.63}$ is an oxygen deficient cubic pyrochlore, similar to that of $Tl_2Os_2O_{7-x}$ but with an enlarged lattice parameter of 10.35128(3) Å compared with 10.29218(3) Å. This is reflected in longer Os–O and A–O bond lengths in the lead derivative. Initially these differences seem inconsistent with the formal osmium oxidation state, based on the use of PbO and the $Os:OsO_4$ starting ratio in the reaction mixture, which was targeted as Os(V). However this calculation assumes that the lead remains as Pb^{2+} during the reaction. Previous work on this material and other lead based precious metal pyrochlores such as $Pb_2Ru_2O_{7-x}$ and $Pb_2Ir_2O_{7-x}$[19] has described both oxygen deficient and stoichiometric forms. In $Pb_2Rh_2O_7$ the observed small lattice parameter of 10.112 Å in comparison with other $Pb_2B_2O_7$ phases has been reported as indicating that this material is correctly written as $Pb^{4+}{}_2Rh^{3+}{}_2O_7$ rather than $Pb^{2+}{}_2Rh^{5+}{}_2O_7$ or $Pb^{2+}Pb^{4+}$-$Rh^{4+}{}_2O_7$. The observed lattice parameter, bond lengths and bond valence sums found in this work, Table 3, also support the idea that $Pb_2Os_2O_{7-x}$ is not a Pb(II)/Os(V) pyrochlore but is better described as $Pb^{2+}{}_{0.63}Pb^{4+}{}_{1.37}Os^{4+}{}_2O_{6.63}$ with mixed lead oxidation states and osmium(IV).

Electronic properties

All three materials reported in this paper show metallic or semimetallic conductivity at room temperature, with resistivities in the range 10^{-2}–10 Ω cm in agreement with literature data on similar materials (summarised in reference 1). Resistivity data obtained for weberite-form $Ca_2Os_2O_7$ over the temperature range 200–450 K are shown in Fig. 6.

The behaviour over this range shows a significant drop in resistivity, about two orders of magnitude, similar to that observed for polycrystalline $Cd_2Os_2O_7$ between 100 and 300 K, with evidence of a weak transition near 300 K again rather

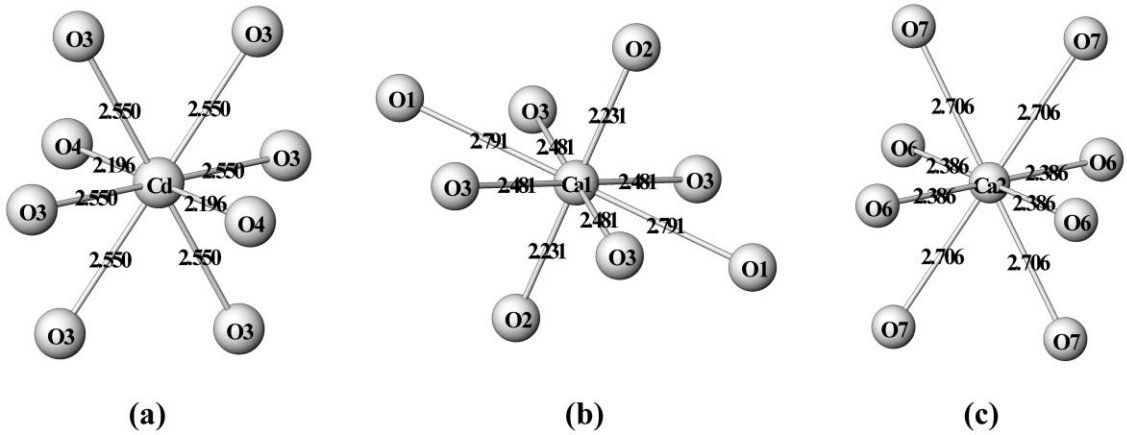

Fig. 5 A-type cation co-ordination environments in (a) pyrochlore and (b) and (c) weberite structures.

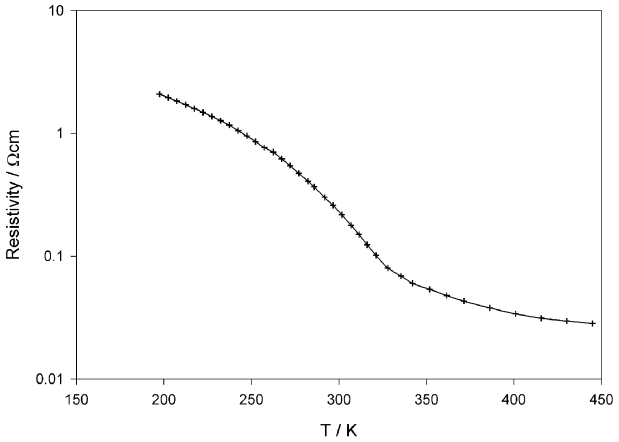

Fig. 6 Resistivity data over the temperature range 150–450 K from weberite form $Ca_2Os_2O_7$.

reminiscent of the $Cd_2Os_2O_7$ data. The variable temperature behaviour below room temperature, with decreasing resistivity, and the absolute values either side of the transition, formally small band gap semi-conductor to poor metallic behaviour, may be indicative of a Slater-like transition. However the resistivity continues to fall slowly between 350 and 450 K, that is the transition in the polycrystalline sample is not to fully metallic behaviour; this may be associated with the low sintering temperature that was necessary to avoid sample decomposition. Attempts to obtain single crystal material suitable for higher quality electronic measurements are in progress, as are measurements of the magnetic properties of this phase to confirm whether the transition is associated with magnetic ordering and thus truly Slater-like.

Results for $Pb_2Os_2O_{7-x}$ were in accord with values previously reported previously by Shaplygin and Lazarev,[18] $\rho \sim 10^{-3}$ Ω cm, while for $Tl_2Os_2O_{7-x}$ the room temperature resistivity datum implies similarities with $Tl_2Ru_2O_{6.5}$.[4]

Conclusions

$Ca_2Os_2O_7$ prepared under ambient pressure conditions is the first osmate found to adopt the weberite structure. Consideration of the relative stabilities of the weberite and pyrochlore structures for $A_2B_2O_7$ systems reported previously indicate that synthesis under higher pressures should lead to formation of the pyrochlore structure for $Ca_2Os_2O_7$, as has indeed been observed by Chamberland.[15] Adoption of the weberite structure with slightly different connectivities in the osmium–oxygen sub-lattice has no significant influence on the electronic properties of this material, *i.e.* both $Cd_2Os_2O_7$ and $Ca_2Os_2O_7$ exhibit poor metallic properties near room temperature. The differences in the connectivities of the BO_6 octahedra are shown in detail in Fig. 7. In both structures chains of vertex sharing octahedra can be considered as being cross-linked by additional octahedra; in pyrochlore these linking units share all vertices and additional oxide ions reside in the channels thus formed while in weberite only four vertices are shared and terminal oxide ions exist. The extensive Os 5d orbitals allow, in the presence of three dimensionally linked OsO_6 octahedra, direct interaction of the osmium centres. While for the pyrochlore systems it seems that the interaction of the Cd and Hg 4 and 5d levels with the Os 5d levels is believed to occur at the Slater transition and be necessary for the metallic regime, this is not so critical for the weberite structure. The origin of this behaviour may lie in the lower symmetry of weberite and would need detailed band structure calculations on this different structure type.

Lead and thallium osmium(IV) oxide pyrochlores may be readily obtained using sealed tube reactions – rather than high pressure techniques as reported previously. Materials formed under these conditions are oxygen deficient and contain a

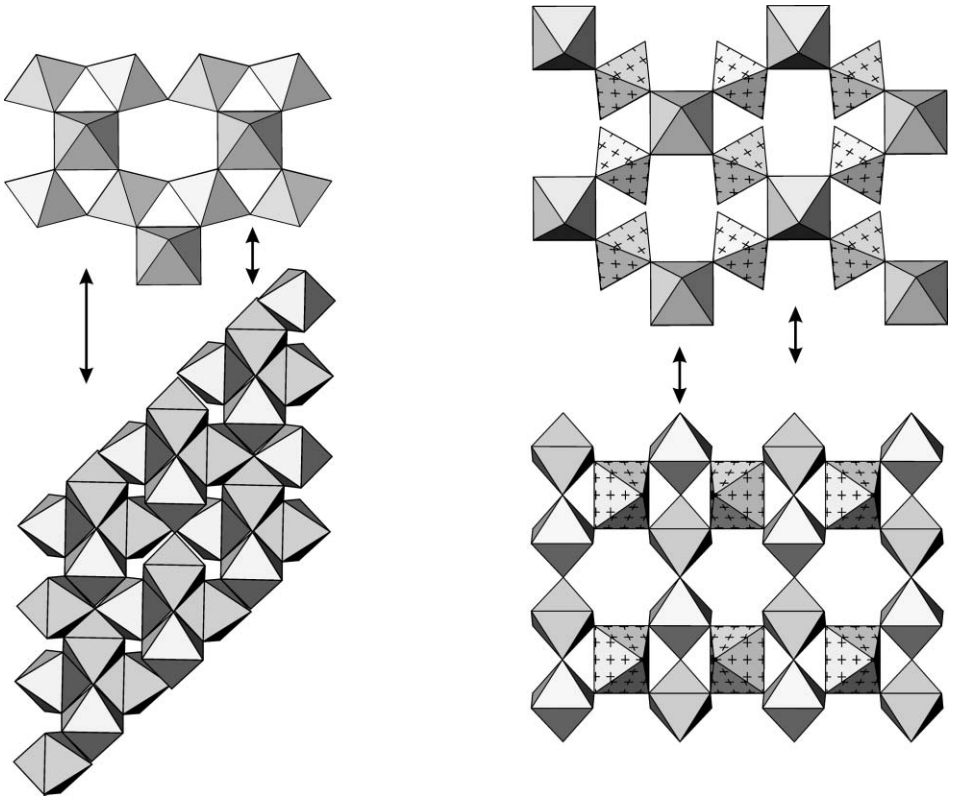

Fig. 7 Polyhedra representations of the pyrochlore (left) and weberite (right) structures. The upper diagrams view the structures along the main channels containing the A-cations. The lower diagrams view the structures perpendicular to this direction showing the different connectivity of the BO_6 octahedra linking the main chains formed from BO_6 octahedra linked through opposite vertices (marked).

mixture of oxidation states on the A-cation site as can be inferred from accurately measured bond lengths. Further definition of the relationship between stoichiometry and electronic properties in these systems, similar to that which has been undertaken for the isoelectronic $Tl_{2-x}Ru_2O_{7-x}$, would obviously be of interest. While $Tl_2Ru_2O_{6.5}$ shows metallic behaviour at room temperature the incorporation of thallium vacancies, as $Tl_{1.8}Ru_2O_7$, or full oxidation, as in $Tl_2Ru_2O_7$, generates materials with metal to insulator transitions at around 100 K.[4]

Acknowledgement

We thank Dr R. Mortimer of DERA, Fort Halstead for help with the resistivity measurements and DERA, also, for the provision of a studentship for J. R.

References

1 M. A. Subramanian, G. Aravamudan and G. V. Subba Rao, *Prog. Solid State Chem.*, 1983, **15**, 55.
2 J. E. Greedan, J. N. Reimers, C. V. Stager and S. L. Penny, *Phys. Rev. B*, 1991, **43**, 5682.
3 B. D. Gaulin, J. S. Gardner, S. R. Dunsiger, Z. Tun, M. D. Lumsden, R. F. Kiefl, N. P. Raju, J. N. Reimers and J. E. Greedan, *Physica B*, 1998, **241–243**, 511.
4 T. Takeda, M. Nagata, H. Kobayashi, R. Kanno, Y. Kawamoto, M. Takano, T. Kamiyama, F. Izumi and A. W. Sleight, *J. Solid State Chem.*, 1998, **140**, 182.
5 H. Sakai, K. Yoshimura, H. Ohno, T. D. Matsuda, H. Kato, S. Kambe, R. Walstedt, Y. Haga and Y. Onuki, *J. Phys. Condens. Matter*, 2001, **13**, L785.
6 I. S. Shaplygin and V. B. Lazarev, *Thermochim. Acta*, 1979, **33**, 225.
7 J. M. Longo, P. M. Raccah, J. A. Kafalas and J. W. Pierce, *Mater. Res. Bull.*, 1972, **7**, 137.
8 W. A. Groen and D. J. W. Ijdo, *Acta Crystallogr., Sect. C*, 1988, **44**, 782.
9 O. Knop, G. Demazeau and P. Hagenmuller, *Can. J. Chem.*, 1980, **58**, 2221.
10 A. W. Sleight, J. L. Gillson, J. F. Weiher and W. Bindloss, *Solid State Commun.*, 1974, **14**, 357.
11 D. Mandrus, J. R. Thompson, R. Gaal, L. Forro, J. C. Bryan, B. C. Chakoumakos, L. M. Woods, B. C. Sales, R. S. Fishman and V. Keppens, *Phys. Rev. B*, 2001, **63**, Article No. 195104.
12 J. Reading and M. T. Weller, *J. Mater. Chem.*, 2001, **11**, 2373.
13 J. Reading, S. Gordeev and M. T. Weller, *J. Mater. Chem.*, 2002, **12**, 1.
14 R. F. Sarkozy and B. L. Chamberland, *Mater. Res. Bull.*, 1973, **8**, 1351.
15 B. L. Chamberland, *Mater. Res. Bull.*, 1978, **13**, 1273.
16 I. S. Shaplygin and V. B. Lazarev, *Thermochim. Acta*, 1977, **20**, 381.
17 A. W. Sleight, *Mater. Res. Bull.*, 1974, **9**, 1177.
18 I. S. Shaplygin and V. B. Lazarev, *Russ. J. Inorg. Chem.*, 1978, **23**, 403.
19 A. W. Sleight, *Mater. Res. Bull.*, 1971, **6**, 775.
20 A. W. Sleight and J. L. Gillson, *Mater. Res. Bull.*, 1971, **6**, 781.
21 A. C. Larson and R. B. von Dreele, *General Structure Analysis System*, Los Alamos National Laboratory, MS-H805, 2000.
22 J. Pannetier and J. Lucas, *Mater. Res. Bull.*, 1970, **5**, 797.
23 D. Altermatt and I. D. Brown, *Acta Crystallogr., Sect B*, 1997, **53**, 135.